Macromolecular Symposia

www.ms-journal.de

Micromagnetic Simulations of Nanoparticles with Varying Amount of Agglomeration

*Tomasz Blachowicz, Jacek Grzybowski, and Andrea Ehrmann**

Magnetic nanoparticles can be used for medical and other purposes, but can also be integrated in polymeric or other nonmagnetic matrices of diverse shapes, for example, thin-films or fibers. In the latter case, it may be important how the magnetic nanoparticles are distributed in the matrix, a topic which is often not taken into account when such composites are investigated experimentally or theoretically. Especially for small magnetic nanoparticles of dimensions allowing coherent reversal, the magnetic properties of such polymer/magnet composites can change drastically in the case of agglomerations. Here, a method is suggested to quantify the influence of nanoparticle distributions inside nonmagnetic matrices. By changing the average distance between nanoparticles of varying diameters between highly distributed particles and perfectly packed clusters, different magnetization dynamics can be modeled by micromagnetic simulations. Here, this process is shown for various magnetic materials and diameter distributions of magnetic nano-spheres and present corresponding micromagnetic simulation results, which underline the importance of taking into account possible magnetic agglomerations in nonmagnetic space.

1. Introduction

Ferromagnetic nanoparticles and nanodots are investigated for diverse applications, for example, in medicine[1–3] or data storage.[4–6] Magnetic nanoparticles are thus produced and investigated by various research groups, focusing on a broad spectrum of materials, going from simple elementary magnets such as iron, cobalt or nickel,[7–9] their oxides, and alloys[10–14] to much more sophisticated magnets such as spinel ferrites.[15,16]

T. Blachowicz, J. Grzybowski
Institute of Physics – Centre for Science and Education
Silesian University of Technology
Gliwice 44-100, Poland

A. Ehrmann
Faculty of Engineering and Mathematics
Bielefeld University of Applied Sciences
33619 Bielefeld, Germany
E-mail: andrea.ehrmann@fh-bielefeld.de

The ORCID identification number(s) for the author(s) of this article can be found under https://doi.org/10.1002/masy.202100381

DOI: 10.1002/masy.202100381

Often, especially simulations are performed on single nanoparticles due to constrictions of time and computing power, while well-defined clusters of magnetic nanodots may exhibit other magnetic properties than the single particles.[17–19]

Much larger problems, however, can be caused by magnetic nanoparticles embedded in a nonmagnetic matrix, such as a polymer, if the position of the nanoparticles is unclear, or it is not known whether these nanoparticles form agglomerations or are well-dispersed. In a previous experiment, we compared transmission electron microscopy (TEM) images of magnetic nanoparticles, embedded in electrospun poly(acrylonitrile) (PAN) nanofibers, and found large differences of the conclusions which could be drawn by these TEM images, varying between apparently fully agglomerated and nearly perfectly separated nanoparticles in different parts of the same nanofiber mat.[20] Choosing different images to perform a micromagnetic simulation of the assumed situation can simply lead to quite different results, which may be highly problematic for the future practical application of such composite fibers. This problem of reproducibility of experimental findings is known under the name "reproducibility crisis"[21,22] and is not only known for highly magnified TEM images,[23] but also for other experimental techniques.[24]

Nevertheless, micromagnetic simulations of varying situations in such a composite, prepared from arbitrarily spaced magnetic nanoparticles in a nonmagnetic matrix, are hard to find in the literature. Schrefl et al. investigated self-assembled FePt nanoparticle arrays, however, for regularly spaced magnetic spheres.[25] Agrawal et al. compared chains and clusters of nickel nanoparticles, without a comparison to smaller clusters or not fully approached nanospheres,[26] while the same group showed the difference between simulations of clusters and single particles.[27] Small systems of 1–4 magnetic permalloy (Py) nanoparticles in different self-assembled cluster geometries were simulated by Kim et al., showing again significant differences between these clusters.[28] Clustering particles of uniaxial and cubic anisotropy, Fidler et al. investigated CoPt and FePt nanoparticles of different diameters between approximately 4 and 80 nm, densely packed in clusters of 1000 nanoparticles, and found a clear influence of the ratio between uniaxial and cubic phases, without investigating the influence of the distance between the nanoparticles in detail.[29]

While these examples underline the importance of investigating the effect of clustering, no systematic approach was found to model different states of clustering, between full agglomerates and perfectly spaced nanoparticles. In our first attempt to examine these effects, we compared ideally distributed nanoparticles with small and larger agglomerates, until all nanoparticles in the simulation were agglomerated.[20] Here, a slightly different approach is chosen, starting from a fully collapsed cluster which are separated to a highly dispersed state, with intermediate states between these extrema to investigate which distances between single nanoparticles cause which effects for different materials.

2. Results and Discussion

To give an impression of what the expansion parameters mean, **Figure 1** gives an overview of the situations under simulation here. The first line shows the situations simulated for 50 nm (Figure 1a–d), followed by 75 nm (Figure 1e–h) and 100 nm (Figure 1i–l).

As these images show, in the densest configuration (expansion ratio = 1) the nanoparticles nearly touch each other after arbitrary positioning inside the given sphere, while an expansion ratio of 8.99 already gives strongly separated nanoparticles without any contact. In this way, it is possible to prepare simulations of more or less agglomerated nanoparticles with arbitrary distribution as an indicator how strongly such differences in the distribution of magnetic nanoparticles in real samples will influence the samples' magnetic properties.

Next, we examine some exemplary hysteresis loops of situations which were simulated in this study. **Figure 2** shows Co nanoparticles with an average diameter of 50 nm, applying the maximum and the minimum concentration combined with expansion ratios of 1 (densely packed), 2.08 as well as 8.99 (maximum expansion rate investigated here). Most of the hysteresis loops show several steps along the slopes of the loops due to single nanoparticle switching their magnetization.

Here, the impact of the expansion ratios is clearly visible. On the one hand, the coercive field increases with increasing expansion rate, that is, in the single particles magnetization reversal is harder than in the clustered ones. On the other hand, the steps which often occur in Co hysteresis loops are nearly vanished for the separated nanoparticles (expansion ratio 8.99), and in this case the hysteresis loops look like typical easy-axis loops. This suggests that the separated nanoparticles, with strongly reduced impact on each other, switch coherently with slightly different coercive fields, as indicated by the small steps visible along the green curves in Figure 2a, b. It should be mentioned that for single magnetic nanoparticles large enough to reverse magnetization via a vortex state (which is typically the case for nanoparticles of diameters 50 nm and larger), most orientations of the external magnetic field show similar hysteresis loops, with a more square hysteresis shape for loops along the easy axis of the particle.[30]

Comparing the different concentrations under investigation, fewer differences are visible. The smaller concentration, that is, the smaller number of magnetic nanoparticles, leads to fewer and more pronounced steps for the smaller expansion ratios (black and red curves in Figure 2a). Differences in the coercive fields are less obvious than in the comparison of the expansion ratios.

Next, **Figure 3** shows the same simulations for iron instead of cobalt. Comparing both materials, the curves clearly differ, which can be attributed to the severe differences in the magnetic properties of both materials, especially the magneto-crystalline anisotropy constants and the cubic (Fe) versus uniaxial (Co) anisotropy (cf. Section 2). For Fe, only small hysteresis loops are visible in addition to areas showing coherent magnetization reversal, as it is often found in magnetic nanoparticles or small agglomerates.

Besides this finding, it is clearly visible that the expansion ratio does not strongly influence the hysteresis curves, which is unexpected since agglomerations might be sufficient to avoid coherent magnetization reversal of the single nanoparticles. This question should be discussed again for larger concentrations, forming larger clusters, which were not under investigation here.

On the other hand, larger average diameters could lead to broader hysteresis loops. This is why **Figure 4** shows simulations of iron nanoparticles for an average particle diameter of 75 nm, also applying higher concentrations. Here, however, the middle parts in which the hysteresis loops open, that is, show irreversible behavior, are not larger than in the previous simulation of 50 nm nanoparticles. Instead, the irreversible part of the hysteresis loop shows a smaller slope, similar to a typical hard-axis loop, for the larger particles. This can easily be understood for coherent magnetization reversal of the whole particles, as it is suggested by the shapes of the hysteresis loops.

Figure 5 presents simulations of nickel nanoparticles of different average diameters. Unexpectedly, the smallest particles show mostly irreversible magnetization curves, with a softer magnetic behavior for the smaller concentration (Figure 5a). For larger particles with average diameters of 75 nm, the hysteresis loops again show smaller slopes, as they are typically found in hard-axis loops, as already found for iron, but also an increased range of reversible change in the magnetization. This effect becomes even more pronounced for the largest average diameters where only a small irreversible hysteresis part is visible within the broad reversible regime.

This at first glance quite unexpected behavior can be explained by the here chosen algorithm to form densely packed agglomerations. As described in Section 2, the dense packing is performed by setting one particle in the middle of the coordinate system and afterward letting the other particles collapse from the outer border of the sphere under examination onto this first particle till they get in contact. As Figure 1i shows, this does not necessarily lead to the densest possible packing, but will leave larger open pores between neighboring nanoparticles than necessitated due to their shape. This plays a role for the possible magnetic coupling between neighboring particles.

Generally, from simulations and measurements of clusters of ferromagnetic nanoparticles, it is well known that stray fields can strongly influence neighboring particles and their respective magnetization reversal processes, even in the case of distances much larger than the exchange length.[31–34] Stray fields are reduced for vortex states, however, while these states are favorable in two-dimensional arrays, the large out-of-plane stray fields along the vortex cores can still influence neighboring particles in a three-dimensional orientation where vortex core orientations can be directed toward neighboring particles. Such interactions can thus generally be expected here for dense packing of

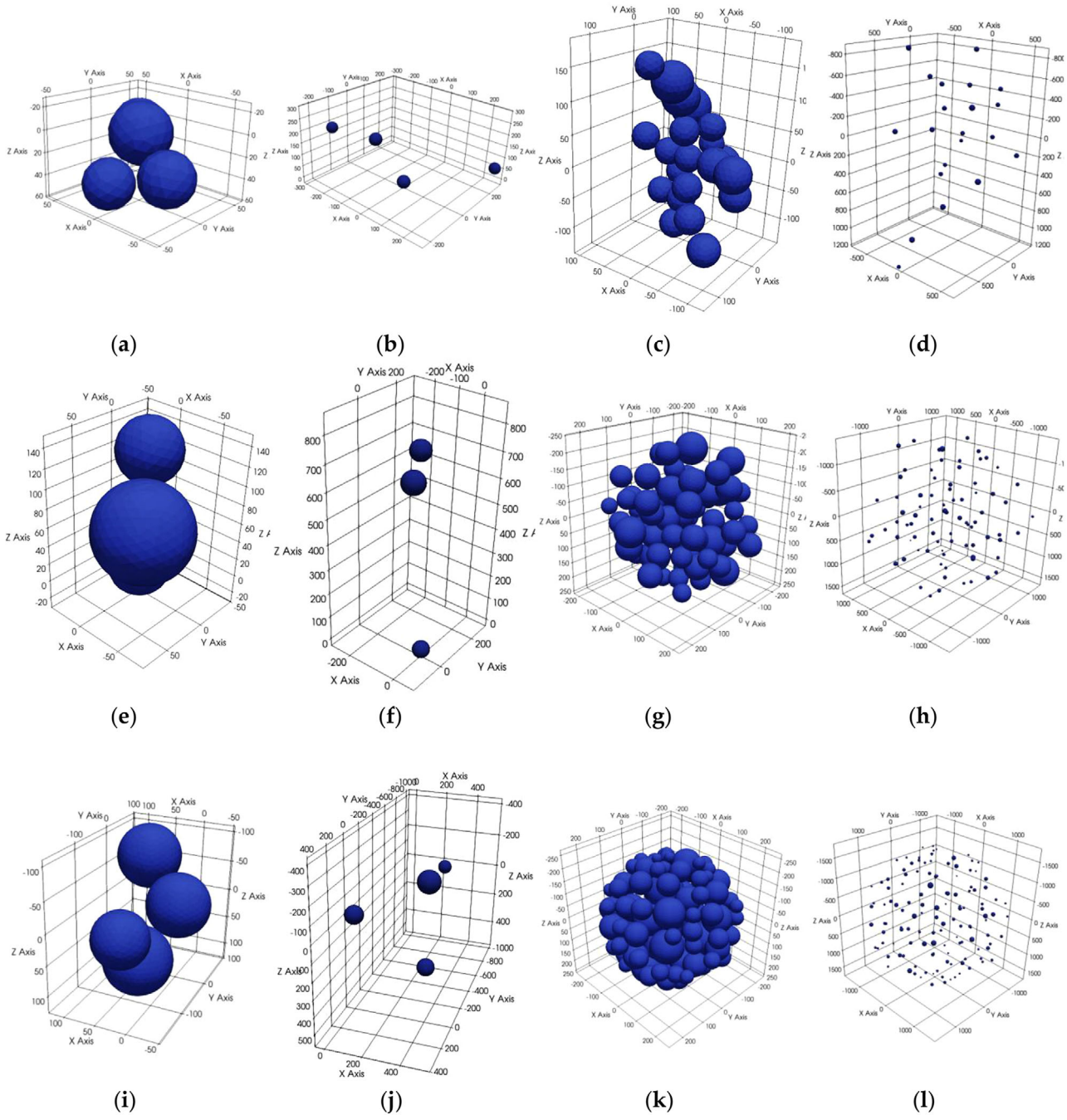

Figure 1. Spheres with varying middle diameters in different concentrations and without expansion ("dense") as well as with an expansion of 8.99 ("expanded"): (a) 50 nm/0.3%/dense; (b) 50 nm/0.3%/expanded; (c) 50 nm/1.75%/dense; (d) 50 nm/1.75%/expanded; (e) 75 nm/0.9%/dense; (f) 75 nm/0.9%/expanded; (g) 75 nm/20%/dense; (h) 75 nm/20%/expanded; (i) 100 nm/2.1%/dense; (j) 100 nm/2.1%/expanded; (k) 100 nm/40%/dense; (l) 100 nm/40%/expanded.

the nanoparticles, independent from the magnetization reversal processes.

As the last material, permalloy (Py) is shown in **Figure 6**, again for the case of 50 nm average diameter. Similar to cobalt, here again the largest expanse factors result in the smoothest hysteresis loops, that is, the lowest magnetic noise, with largest coercive fields. The open hysteresis loops in spite of vanishing magnetocrystalline anisotropy are usually attributed to the interplay between interparticle interaction and magnetization distribution inside the particles.[35] Such effects were also found in other micromagnetic and experimental studies of Py rings,[36,37] where the coercive fields were larger than zero due to switching from onion into vortex states instead of coherent magnetization rotation, and in Py disks which were large enough to form a vortex state,[38]

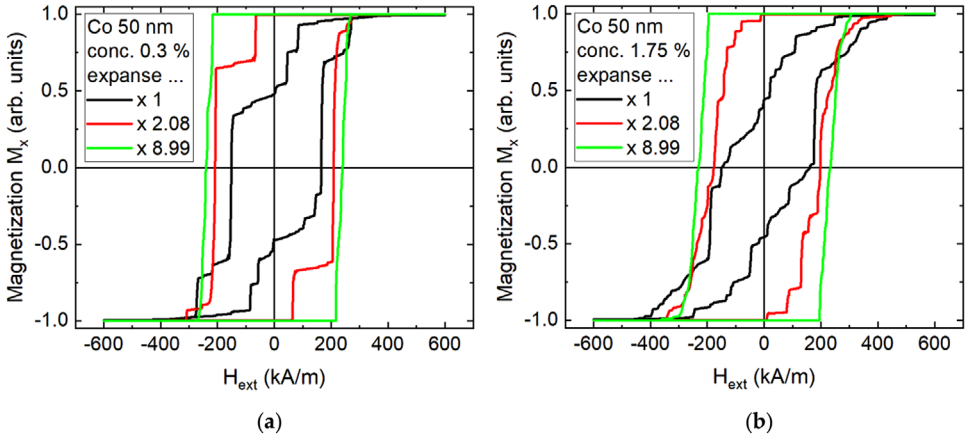

Figure 2. Cobalt nanoparticles of diameter 50 nm in different expansion rates for the concentrations (a) 0.3%; (b) 1.75%.

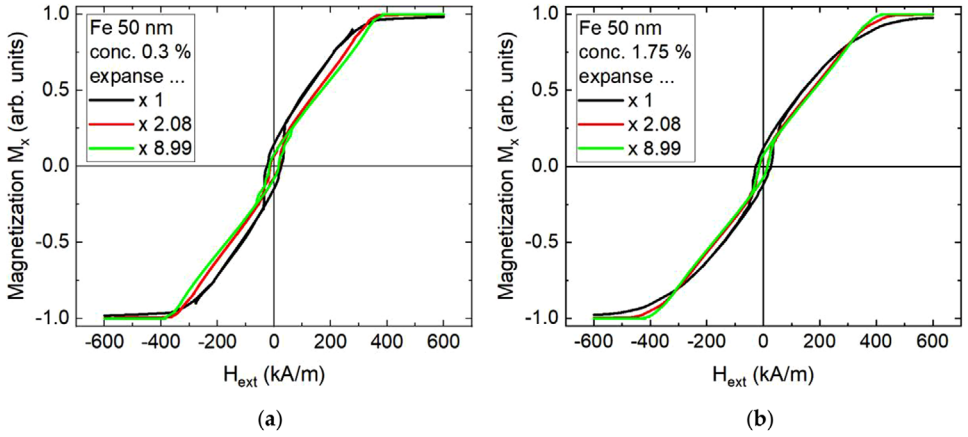

Figure 3. Iron nanoparticles of diameter 50 nm in different expansion rates for the concentrations (a) 0.3%; (b) 1.75%.

where the hysteresis loop shows irreversible parts due to vortex nucleation and annihilation. It should be mentioned that while vortex formation is often visible by a reversible part of the hysteresis loop near zero field, this is not the case if the vortex forms only after reversing the external magnetic field.

Unexpectedly, in some hysteresis loops a clear asymmetry is visible, as it is usually only found in exchange bias systems[39,40] or also in special nanostructures in which magnetically hard and soft areas are realized by the shape anisotropy.[41] This effect is especially visible for the low concentration (Figure 6a) and can be

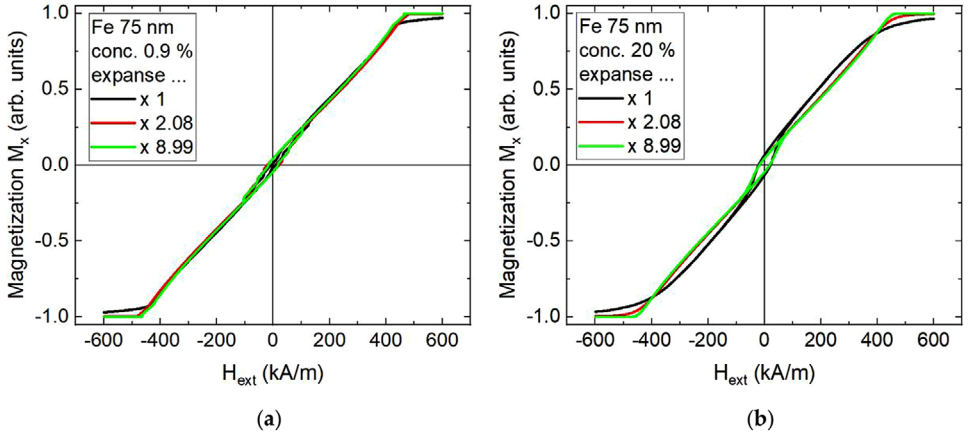

Figure 4. Iron nanoparticles of diameter 75 nm in different expansion rates for the concentrations (a) 0.9%; (b) 20%.

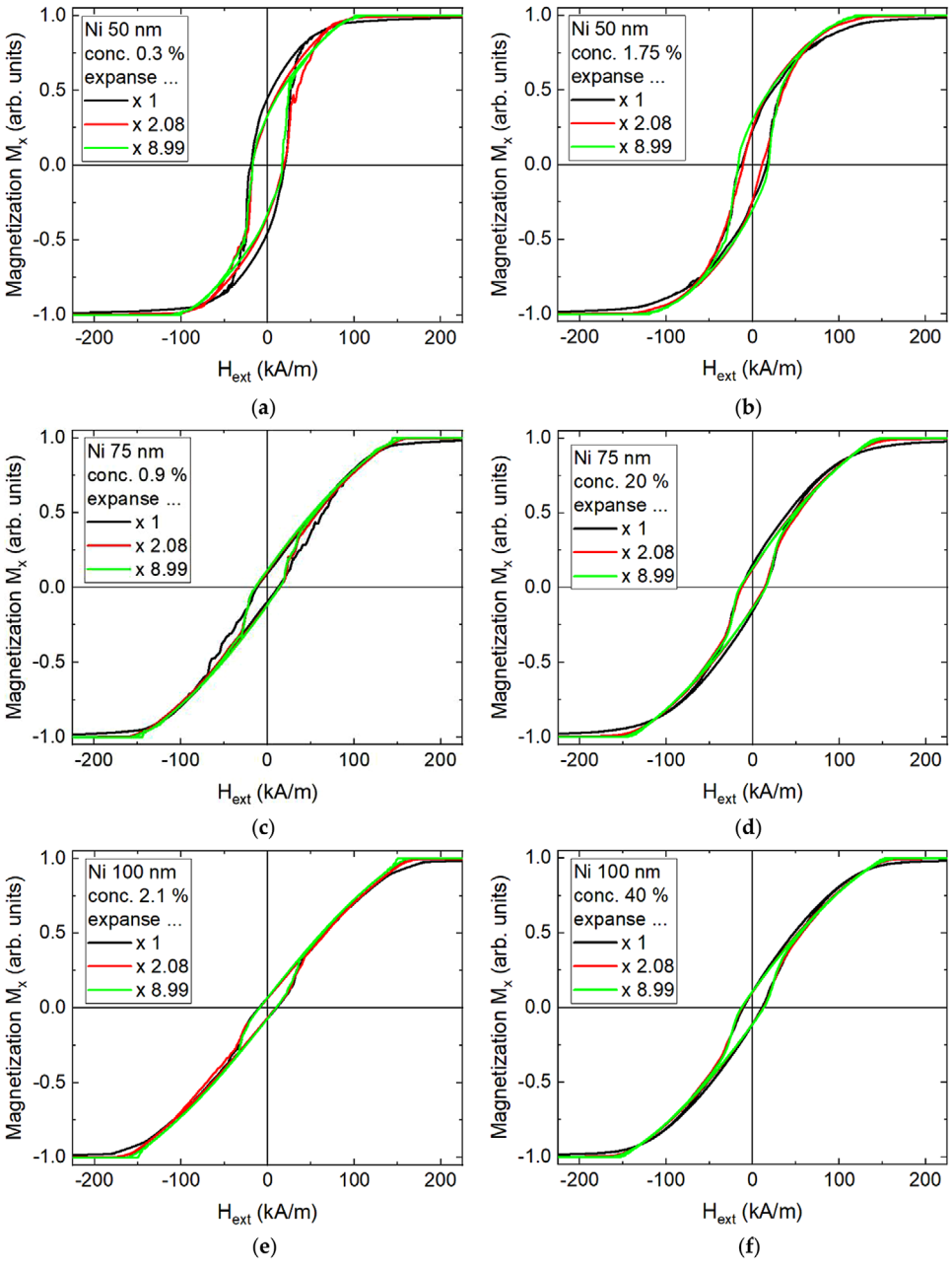

Figure 5. Nickel nanoparticles in various expansion rates for the diameters and concentrations (a) 50 nm/0.3%; (**b**) 50 nm/1.75%; (a) 75 nm/0.9%; (b) 75 nm/20%; (e) 100 nm/2.1%; (f) 100 nm/40%. x-axis values differ from previous plots.

explained by a certain randomness inherent in the Magpar calculations, leading to magnetic noise. It shows how fragile magnetization reversal in these nanostructures is for some materials, indicating a reduced reliability of these structures in real applications.

Finally, **Figure 7** shows the concentration-dependent coercive fields for the four materials under examination here. For Fe and Ni, the coercive are more or less independent from the concentration as well as from the expansion ratio, as visible for all nanoparticle dimensions. For Co, we also see that the coercive fields are similar for all concentrations and nanoparticle diameters under examination here, while the expansion ratio clearly influences the coercive fields. For the 100 nm nanoparticles with a concentration of 2.1%, there is an outlier visible at an expansion ratio of 1.28; besides this value, there is a general trend visible to have larger coercive fields for larger expansion ratios, with the coercive fields reaching saturation at a ratio of ~1.3. An even more pronounced effect is visible for permalloy (Figure 7d), the material with the largest exchange length, in the case of the smallest diameters, while nearly no dependence of the coercive field on the expansion ratio is visible for 100 nm particles with a concentration of

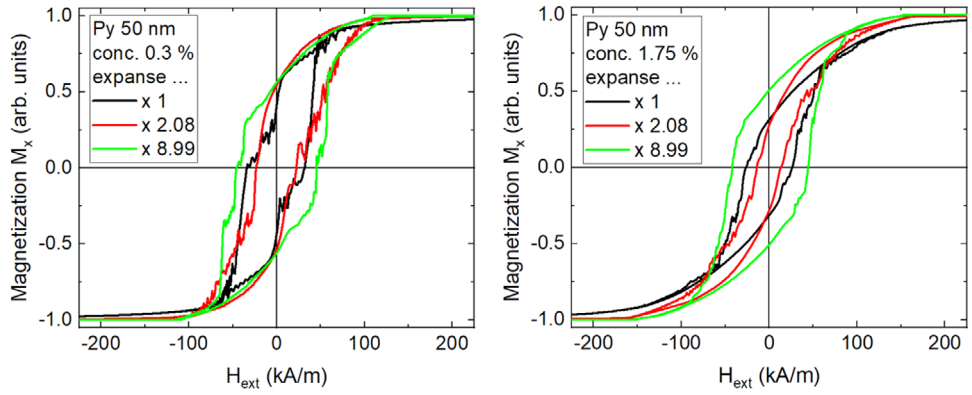

Figure 6. Permalloy nanoparticles of diameter 50 nm in different expansion rates for the concentrations (a) 0.3%; (b) 1.75%.

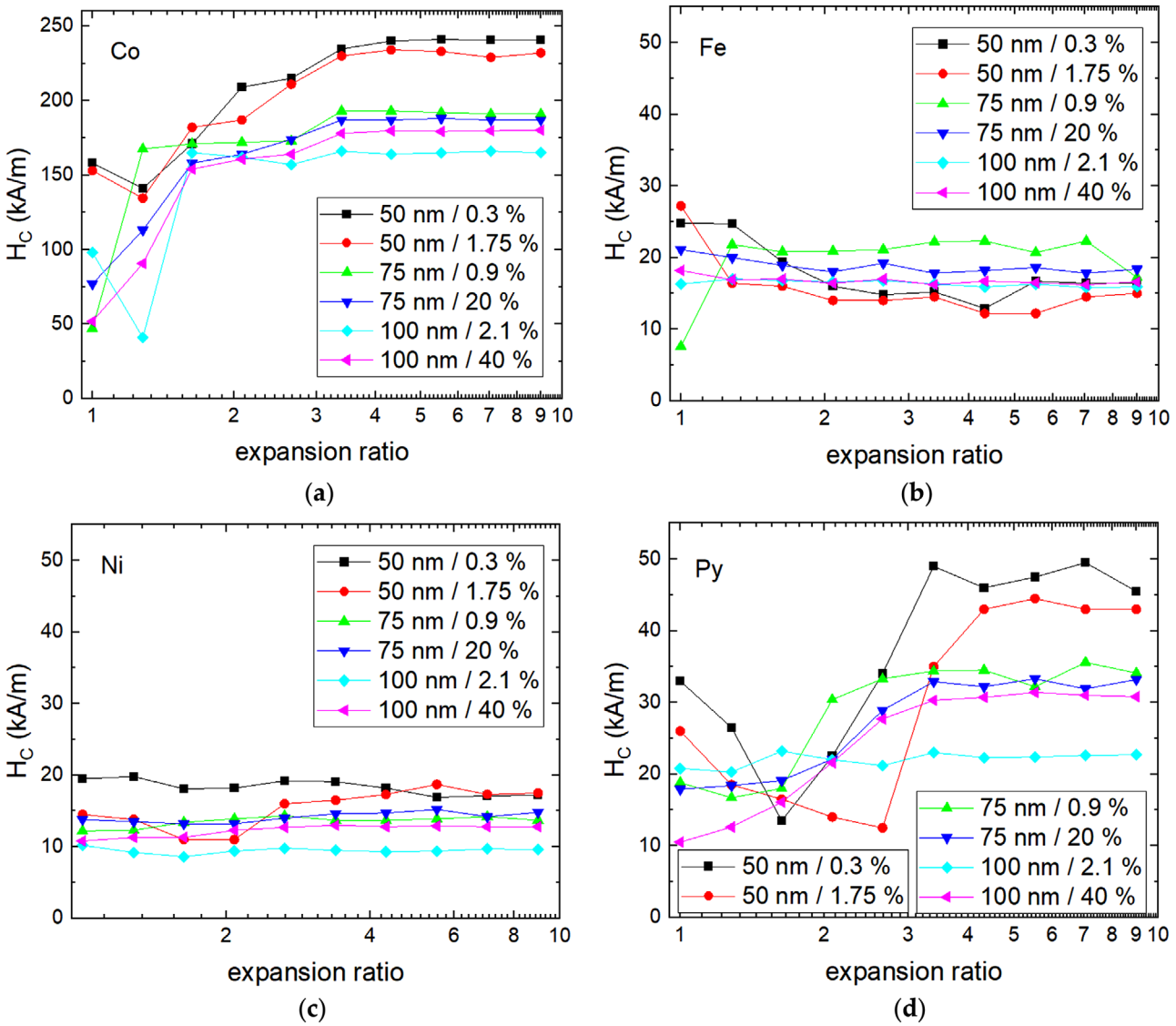

Figure 7. Concentration-dependent coercive fields for (a) cobalt; (b) iron; (c) nickel; and (d) permalloy. The y-axis of (a) differs from the others.

2.1%. No trend valid for all materials under investigation can be reported.

In general, this study shows that for some materials the magnetic properties are significantly influenced by the distribution of the identical amount of nanoparticles in a given area. This impact seems to be larger for materials with larger exchange lengths. This idea fits well to a previous study dealing with magnetite and nickel ferrite,[20] materials with even larger exchange length in the range of 27 nm (magnetite) or 10 nm (nickel ferrite), respectively,[42,43] where especially for magnetite severe differences between fully agglomerated and distributed nanoparticles were found. Unexpectedly, the influence of the concentration is relatively low in most cases. Again, for permalloy it seems to be the highest, suggesting further investigations of the same constellation prepared with magnetite.

It must be mentioned that an experimental evaluation of expansion ratio-dependent coercive fields is nearly impossible since usually, when measuring the magnetic properties of a polymer/nanoparticle composite, only the overall nanoparticle content is known, not its distribution. While the general effect of the average distance between neighboring nanoparticles can be experimentally verified, for example, by carbonizing a PAN matrix in which magnetic nanoparticles are embedded,[44] a method detecting the magnetic properties with high spatial resolution (such as magnetic force microscopy) in combination with a method detecting the nanoparticles at the same position (such as EDX) would be necessary for a more detailed evaluation. Our simulations can thus be treated as a hint that modeling such systems with embedded magnetic nanoparticles is only reliable if the content distribution is measured at several positions and the simulation is fitted to this content distribution, instead of simply working with the average content.

3. Conclusion

A program was developed enabling modeling arbitrary distributions of nanoparticles in a given sphere with a defined expansion ratio, here shown between 1 (fully agglomerated in the meaning that no nanoparticle can be shifted nearer to the middle of the sphere without changing its spherical angles) and 8.99.

These models were used to show the impact of this expansion ratio on the magnetic properties of the whole system. Especially for permalloy, a strong impact of the expansion ratio was found for both concentrations of magnetic material investigated here, while Fe and Ni showed nearly identical coercive fields for different expansion ratios. This impact was also found in previous investigations of magnetite and nickel ferrite and may be correlated with the exchange lengths of the materials, which are the largest for magnetite, nickel ferrite, and permalloy, and the smallest for iron which shows only a weak dependence of the coercive fields on the expansion ratios.

In the future, it is necessary to model more materials with the newly developed program to give a broader overview of the material-dependent influence of agglomerations in magnetic/nonmagnetic composites and to add temperature-dependent simulations for more realistic comparison with the experiment.

4. Experimental Section

Micromagnetic simulations were performed by the micromagnetic solver Magpar, working by solving the Landau–Lifshitz–Gilbert equation of motion.[45] The simulated materials were Py, Fe, Ni, and Co with the model parameters given in **Table 1**. These materials were chosen as the starting point since they were commercially available as nanoparticles and thus of practical interest for many research groups, while they offered a broad range of anisotropy constants and other magnetic parameters. The easy anisotropy axes were oriented along the x-axis so that in the case of highly agglomerated systems, square hysteresis loops can be expected.

The process of cluster formation was performed as follows. In a given nonmagnetic sphere of diameter 540 nm, sphere-shaped nanoparticles of defined diameter normal distributions with typical averages of 50, 75, and 100 nm and given standard deviations of 8.3, 12.5, and 16.7 nm, respectively, were embedded. The number of magnetic spheres was defined by a concentration, as it would be done practically in the preparation of a composite of magnetic nanoparticles in a nonmagnetic matrix. Concentrations were assumed of 0.3% and 1.75% for the 50 nm case, 0.9% and 20% for the 75 nm case, and 2.1% and 40% for the 100 nm case. It must be mentioned that these concentrations were averaged over the whole spheres, with the nanoparticles not being distributed normally, but as described below.

Starting from arbitrary positions of all nanoparticles in the sphere, first full agglomeration was produced by letting the distance of each nanoparticle to the center of the nonmagnetic sphere shrink until neighboring nanoparticles touched each other (without changing a particle's spherical angles, that is, the particle stayed on the connection line between its center and the center of the whole simulation sphere, and only the distance to the center of the simulation sphere was modified). Oppositely, expansion was performed by increasing the distance of each nanoparticle to the center of the sphere in fully agglomerated state by a factor, for example, of 1.28, 1.63, 2.08, etc. Here, simulations were shown with different expansion ratios between 1 (i.e., agglomerated cluster) and 8.99, modeling hysteresis loops with the external magnetic field were sweeping along the x-axis. In this way, the interactions between neighboring particles were modified, thus modifying the magnetic properties of the overall system. It must be mentioned that for the largest expansion ratios, the original sphere of diameter 540 nm was no longer limit the positions of the particles so that the original concentrations, related to the original sphere, were no longer valid for a simulation space without fixed borders. Nevertheless, to definitely reach a saturated state in which the coercive fields did not change with further increasing distances between neighboring nanoparticles, it was necessary to cross the original sphere's space borders.

Table 1. Model parameters of simulated materials.

Parameter	Py	Fe	Ni	Co
Anisotropy constants	$K_1 = 0.0$	$K_1 = 4.8 \cdot 10^4$ J m^{-3}, $K_2 = 5.0 \cdot 10^3$ J m^{-3}	$K_1 = -4.8 \cdot 10^3$ J m^{-3}	$K_1 = 5.3 \cdot 10^5$ J m^{-3}
Exchange constant A	$1.3 \cdot 10^{-13}$ J/m	$2.0 \cdot 10^{-11}$ J m^{-1}	$3.4 \cdot 10^{-12}$ J m^{-1}	$1.03 \cdot 10^{-11}$ J m^{-1}
Magnetic polarization at saturation J_S	1.005 T	2.1 T	0.61 T	1.76 T
Gilbert damping constant α	0.02	0.1	0.1	0.01

Acknowledgements

Research efforts were partially supported (T. B.) by the Silesian University of Technology Rector's Grant no. 14/030/RGJ21/00110.

Conflict of Interest

The authors declare no conflict of interest.

Data Availability Statement

The data that support the findings of this study are available from the corresponding author upon reasonable request.

Keywords

iron, collapse, cross-section, permalloy, spherical coordinates, virtual sphere

Received: September 21, 2021
Revised: December 20, 2021

[1] R. Barbucci, D. Pasqui, G. Giani, M. De Cagna, M. Fini, R. Giardino, A. Atrei, *Soft Matter* **2011**, *7*, 5558.
[2] Y. Slimani, B. Unal, E. Hannachi, A. Selmi, M. A. Almessiere, M. Nawaz, A. Baykal, I. Ercan, M. Yildiz, *Ceram. Int.* **2019**, *45*, 11989.
[3] A. F. Abu-Bakr, A. Yu Zubarev, *Eur. Phys. J. Spec. Top.* **2020**, *229*, 323.
[4] G. Reiss, A. Hütten, *Nat. Mater.* **2005**, *4*, 725.
[5] S. Gliga, M. Yan, R. Hertel, C. M. Schneider, *Phys. Rev. B* **2008**, *77*, 060404(R).
[6] B. Poornaprakash, S. Ramu, K. Subramanyam, Y. L. Kim, M. Kumar, M. S. P. Reddy, *Ceram. Int.* **2021**, *47*, 18557.
[7] M. Ghazvini, H. Maddah, R. Peymanfar, M. H. Ahmadi, R. Kumar, *Phys. A: Stat. Mech. Appl.* **2020**, *551*, 124127.
[8] P. Sharma, N. Holliger, P. H. Pfromm, B. Liu, V. Chikan, *ACS Omega* **2020**, *5*, 19853.
[9] M. R. Ahghari, V. Soltaninejad, A. Maleki, *Sci. Rep.* **2020**, *10*, 12627.
[10] G. Rana, P. Dhiman, A. Kumar, D.-V. N. Vo, G. Sharma, S. Sharma, Mu. Naushad, *Chem. Eng. Res. Des.* **2021**, *175*, 182.
[11] A. Ghosh, V. Srinivas, R. Sundara, *J. Alloys Compd.* **2020**, *818*, 152931.
[12] N. Mohamed, O. E. A. Hessen, H. S. Mohammed, *Inorg. Chem. Commun.* **2021**, *128*, 108572.
[13] K. Tanbir, M. P. Ghosh, R. K. Singh, M. Kar, S. Mukherjee, *J. Mater. Sci.: Mater. Electron.* **2020**, *31*, 435.
[14] P. A. Vinosha, A. Manikandan, R. Ragu, A. Dinesh, K. Thanrasu, Y. Slimani, A. Baykal, B. Xavier, *J. Alloys Compd.* **2021**, *857*, 157517.
[15] Y. Slimani, M. A. Almessiere, M. Sertkol, S. E. Shirsath, A. Baykal, M. Nawaz, S. Akhtar, B. Ozcelik, I. Ercan, *Ultrason. Sonochem.* **2019**, *57*, 203.
[16] Y. Slimani, B. Unal, M. A. Almessiere, A. D. Korkmaz, S. E. Shirsatz, G. Yasin, A. V. Trukhanov, A. Baykal, *Results Phys.* **2020**, *17*, 103061.
[17] A. Remhof, A. Schumann, A. Westphalen, T. Last, U. Kunze, H. Zabel, *J. Magn. Magn. Mater.* **2007**, *310*, e794.
[18] X. S. Gao, L. F. Liu, B. Birajdar, M. Ziese, W. Lee, M. Alexe, D. Hesse, *Adv. Funct. Mater.* **2009**, *19*, 3450.
[19] D. Sudsom, A. Ehrmann, *Nanomaterials* **2021**, *11*, 349.
[20] M. Wortmann, A. S. Layland, N. Frese, U. Kahmann, T. Grothe, J. L. Storck, T. Blachowicz, J. Grzybowski, B. Hüsgen, A. Ehrmann, *Sci. Rep.* **2020**, *10*, 14708.
[21] M. Baker, *Nature* **2016**, *533*, 452.
[22] National Academies of Sciences, Engineering, and Medicine, *Reproducibility and Replicability in Science*, National Academies Press, Washington **2019**.
[23] P. M. Anderson, H. Guo, P. B. Sunderland, *J. Aerosol Sci.* **2017**, *114*, 317.
[24] M. R. Linford, et al., *Microsc. Microanal.* **2020**, *1*, 1.
[25] T. Schrefl, G. Hrkac, D. Suess, W. Scholz, J. Fidler, *J. Appl. Phys.* **2003**, *93*, 7041.
[26] M. Agrawal, B. Rana, A. Barman, *J. Phys. Chem. C* **2010**, *114*, 11115.
[27] B. Rana, M. Agrawal, S. Pal, A. Barman, *J. Appl. Phys.* **2010**, *107*, 09B513.
[28] M.-K. Kim, P. Dhak, H.-Y. Lee, J.-H. Lee, M.-W. Yoo, J. H. Lee, K. S. Jin, A. Chu, K. T. Man, H. S. Park, S. Aizawa, T. Tanigaki, D. Shindo, M. Y. Kim, S.-K. Kim, *Appl. Phys. Lett.* **2014**, *105*, 232402.
[29] J. Fidler, P. Speckmayer, T. Schrefl, D. Suess, *J. Appl. Phys.* **2005**, *97*, 10E508.
[30] N. A. Usov, M. S. Nesmeyanov, V. P. Tarasov, *Sci. Rep.* **2018**, *8*, 1224.
[31] V. L. Mironov, E. V. Skorohodov, J. A. Blackman, *J. Appl. Phys.* **2014**, *115*, 184301.
[32] A. Sukhov, P. P. Horley, J. Berakdar, A. Terwey, R. Meckenstock, M. Farle, *IEEE Trans. Magn.* **2014**, *50*, 1.
[33] M. D. Costa, Yu. G. Pogorelov, *Phys. Stat. Sol. A* **2001**, *189*, 923.
[34] A. Ehrmann, T. Blachowicz, *J. Nanomater.* **2017**, *2017*, 5046076.
[35] A. A. Fraerman, S. A. Gusev, L. A. Mazo, I. M. Nefedov, Y. U. N. Nozdrin, I. R. Karetnikova, M. V. Sapozhnikov, I. A. Shereshevskii, L. V. Sukhodoev, *Phys. Rev. B* **2002**, *65*, 064424.
[36] M.-F. Lai, Y.-J. Chen, D.-R. Liu, C.-K. Lo, C.-J. Hsu, C.-N. Liao, C.-P. Lee, Y.-H. Chiu, Z.-H. Wei, *IEEE Trans. Magn.* **2010**, *46*, 179.
[37] M.-F. Lai, Z.-H. Wei, C.-R. Chang, J. C. Wu, J. H. Kuo, J.-Y. Lai, *Phys. Rev. B, Condens. Matter* **2003**, *67*, 104419.
[38] P. Vavassori, M. Grimsditch, V. Metlushko, N. Zaluzec, B. Ilic, *Appl. Phys. Lett.* **2005**, *86*, 072507.
[39] J. Nogués, I. K. Schuller, *J. Magn. Magn. Mater.* **1999**, *192*, 203.
[40] T. Blachowicz, A. Ehrmann, *Coatings* **2021**, *11*, 122.
[41] J. Detzmeier, K. Königer, T. Blachowicz, A. Ehrmann, *Nanomaterials* **2021**, *11*, 800.
[42] Y. Zhang, Z. Y. Ren, Y. Fu, X. Yuan, Y. Zhai, H. B. Huang, H. R. Zhai, *J. Phys. Chem. Solids* **2009**, *70*, 505.
[43] J. B. Zhang, R. W. Shu, C. L. Guo, R. R. Sun, Y. Chen, J. Yuan, *J. Alloys Comp.* **2019**, *784*, 422.
[44] N. Fokin, T. Grothe, A. Mamun, M. Trabelsi, M. Klöcker, L. Sabantina, C. Döpke, T. Blachowicz, A. Hütten, A. Ehrmann, *Materials* **2020**, *13*, 1552.
[45] W. Scholz, et al., *Comput. Mater. Sci.* **2003**, *28*, 366.